

Dispersal and organization of polarized cells: non-linear diffusion and cluster formation without adhesion

G. Nakamura, M. Badoual, E. Fabiani, and C. Deroulers*

Université Paris-Saclay, CNRS/IN2P3, IJCLab, 91405 Orsay, France and

Université de Paris, IJCLab, 91405 Orsay, France

Abstract

Experimental studies of cell motility in culture have shown that under adequate conditions these living organisms possess the ability to organize themselves into complex structures. Such structures may exhibit a synergy that greatly increases their survival rate and facilitate growth or spreading to different tissues. These properties are even more significant for cancer cells and related pathologies. Theoretical studies supported by experimental evidence have also shown that adhesion plays a significant role in cellular organization. Here we show that the directional persistence observed in polarized displacements permits the formation of stable cell aggregates in the absence of adhesion, even in low-density regimes. We introduce a discrete stochastic model for the dispersal of polarized cells with exclusion and derive the hydrodynamic limit. We demonstrate that the persistence coupled with the cell-cell exclusion hinders the cellular motility around other cells, leading to a non-linear diffusion which facilitates their capture into larger aggregates.

* derouler@ijclab.in2p3.fr

The organization of living organisms into structures with complex patterns remains an intriguing problem in cell biology [1]. Even more so if the resulting structures exhibit enhanced properties that alters the normal functioning of healthy tissues and their surroundings, or even damage them as a byproduct of their metabolism. That is often the case for cancer cells which form abnormal tissues with pathological properties such as uncontrolled cellular growth or metastatic dissemination [2, 3]. Metastasis involves the ability to migrate away from the primary tumor to secondary sites in healthy tissue, either in an individual or collective level, and constitute an important aspect of cancer research. This phenomenon belongs to a broader class described by migration and displacement of cells [4]. Other important examples include wound healing [5] and bacterial swarm [6–8].

Unfortunately, the precise details of collective cell dynamics remains unclear at this point due to the rich framework of interactions mediated by cell-cell junctions, adhesion molecules, or emergent dynamical phenomena [9]. For instance, it has been observed experimentally that directional persistence prompts coordinated migration patterns even in the absence of cell-cell junctions in low-dimensional systems [10], striking the stance that explicit interactions are necessary for collective motions of cells. On the other hand, our understanding of the molecular and biological processes responsible for the movement of isolated cells have vastly improved in the past decade [9, 11, 12]. The various sorts of cell movement and their frequencies depends, naturally, on the morphology of the tissue in question. In the case of glial cells – the non-neuronal cells in the nervous system – their high mobility can lead to a very aggressive type of cancer shall they evolve into tumor cells (glioma) [13]. As the cancer cells infiltrate into the healthy tissue, the spatial boundaries that delimit the tumor become more diffuse and ultimately reduce the likelihood of complete removal of the tumor by surgical interventions. The displacement of isolated glioma cells occurs through polarization, a mechanism that reorganizes the inner components of the cell and favors the displacement along a given direction via action of myosin II [14, 15]. Polarization confers glioma cells the ability to elongate their bodies along a given direction and cross narrow intercellular spaces and thus travel long distances inside the brain parenchyma. The elongation can be interpreted as a morphological change via actin waves [16], that orients the traction and retraction of the cell membrane. The long-lasting nature of the polarization favors the persistence of cell movements and produces an average directional migration thanks to correlations between consecutive displacements [17].

Migration of polarized cells consists of the repetition of three steps. First, the cell polarizes along a given direction. It then moves along that direction until it eventually comes to a rest; and finally it depolarizes restoring its original shape. In the absence of environmental bias, the polarization direction is chosen randomly which confers an erratic aspect to the cell migration. More specifically, the migration of polarized cells describes a velocity jump stochastic process in the category of the correlated random walker [18]. Adhesion and exclusion – the most prominent cell-cell interactions – arise as more and more cells are brought into contact with increasing cell concentrations. Adhesion encompasses the short range attractive forces that are exchanged between neighbouring cells via cell-cell junctions and other adhesion molecules. Exclusion summarizes the inability of any two different cells to share the same position at the same time. In practice, exclusion also reduces the overall cellular mobility as cells become obstacles for displacements, but it does not create, at least for cells, a net repulsive force. As a result, cell-cell interactions tend to further reduce the motility of cells in regions with elevated cellular concentrations inducing a self-trapping effect. The process triggers the aggregation of cells and separates the system into two co-existing phase, namely, a gas phase formed by diluted cells and a liquid phase comprised of large clusters. By now it is well-known that this phenomenon describes the motility-induced phase separation (MIPS) and occurs for self-propelled particles (SPP) even in absence of adhesive forces [19–22]. New phenomenology in MIPS has been unveiled including the ability to create topological defects populated with bubbles for 2D active Brownian particles (ABP) [23], breakdown of MIPS with anisotropic SPP [24], and emergence of spontaneous velocity alignment forces [25]. The connection between MIPS and velocity alignment interactions – whose foundations stem from the seminal work of Vicsek [26] – connects two branches of active matter physics [27, 28] characterized by different types of phase transition. The former usually invokes first-order phase transitions to create the phase separation in out-of-equilibrium systems due to particle and/or temperature imbalance [29], while the later employs the rapid transmission of fluctuations across particles in continuous phase transitions as a way to sustain the information flow required for self-organization [30, 31]. Lattice-gas particles with non-convex shapes such as crosses suppress rotations and induce persistence. At high levels of persistence, regions without particles are observed creating a rich nonequilibrium phase diagram [32].

Here we formulate a discrete ABP model for polarized cells based on the typical pat-

terns observed in cellular migration. The growth rate is assumed to be negligible either by considering short time intervals or by chemical suppression. We limit cell-cell interactions to exclusion effects in order to examine the interplay between polarization and cell density and their effects on cellular organization. Similar premises were also considered before: in absence of depolarization of cells before direction changes in [33], and in the ballistic regime for diluted systems [34]. Migration of cancer cells with adhesion has been addressed before and compared with experiments on gap junctions [35] and on formation of deformable aggregates with proliferation [36]. More recently, a data-driven model has shown that the density-dependent propulsion with adhesion promotes the rotation of the clusters of cancer cells [37]. In [38], the authors investigate the role of adherens junctions and constraints of the extracellular matrix on cell migration and jamming transitions. More specifically, by deregulating the expression of E-cadherin they study the transition between collective and individual cell migration and tissue invasion in human breast carcinoma. Starting from our bottom-up approach, Monte Carlo simulations show that cells self-organize into two phases (gas and liquid) with distinct properties, with particles being exchanged according to a power-law. Furthermore, we obtain the mean-field diffusion equation for the gas phase and demonstrate that the diffusion coefficient acquires negative values near the gas-liquid interface. The paper is organized as follows. Sec. I introduces the model and parameters for polarized cells. The master equation and relaxation time of global quantities are described in Sec. II. Self-jamming drives nucleation and aggregation of cells into large clusters even in low-density regimes. We describe the phenomenon in Sec. III. The effective diffusion coefficient of the gas-like phase is derived and compared with simulated data in Sec. IV, with concluding remarks in Sec. V.

I. MODEL

The model describes the displacement of N cells placed in the sites of a regular square lattice in d dimensions (see Fig. 1) with volume $V = L^d$ and orthonormal basis $\{\mathbf{e}_1, \mathbf{e}_2, \dots, \mathbf{e}_d\}$. The lattice spacing a is taken to a microscopic length scale of the order of the typical size of cells. For glioma cells, this scale falls between 20–40 μm , although the actual value is immaterial for our theory. Each site support at most one cell, and each cell can be found in the non-polarized state or in one of the $2d$ available polarization states. For the sake

TABLE I. Parameter description.

γ	displacement rate
Λ	polarization rate
Γ	depolarization rate

of convenience, we associate the non-polarized state with the null vector $\mathbf{e}_0 = \vec{0}$ while the polarized ones are either parallel or anti-parallel to coordinate versors, $\mathbf{p}_{\pm k} = \pm \mathbf{e}_k \equiv \mathbf{e}_{\pm k}$. Non-polarized cells lack discernible mobility and remain in place for $1/\Gamma$ units of time in average. Γ is the polarization rate of the transition from the non-polarized state to polarized one, and whose direction is sampled from a uniform distribution. Polarized cells revert to the non-polarized state with depolarization rate Λ or, equivalently, after a typical time interval $1/\Lambda$. The correlated displacement requires that cells with polarization \mathbf{p}_k can only move along the same direction by $a\mathbf{e}_k$ into the next empty neighbouring site, with movement rate γ . Furthermore, we assume the time step δt is short enough so that multiple single cell transitions become unlikely. The initial placement of cells follows a uniform distribution with cells polarized in the direction \mathbf{e}_1 . Table I summarizes the transition rates.

Given the aforementioned requirements and stochastic rules, one can implement a simple cellular automaton on a square lattice to produce numerical simulations. Unless stated otherwise, we also assume periodic boundary conditions. The cellular automaton goes as follows. Each time step comprises N consecutive updates of a random sequence formed by N cells. The random sampling of cells, repetitions included, reduces eventual biases caused by improper exploration of the phase space (excluding repetitions would reduce the relaxation time for certain global statistics such as the concentration of non-polarized cells).

Once a cell is selected, one generates a random number $x \in [0, 1)$ from a uniform distribution. What happens next depends on the polarization state of the selected cell. Non-polarized cells polarize for $x < (\Gamma\delta t)e^{-\Gamma\delta t} \approx \Gamma\delta t$. The new polarization state is obtained by sampling the polarization direction from a uniform distribution. On the other hand, polarized cells may either move along the polarization axis for $x < \gamma\delta t$ as long as the target site is vacant; or depolarize if $\gamma\delta t \leq x < (\gamma + \Lambda)\delta t$. It is worth noting that the time interval δt used for single cells appears in all expressions involving probabilities. Thus, we can tune the automaton by enforcing that polarized cells always perform an action within

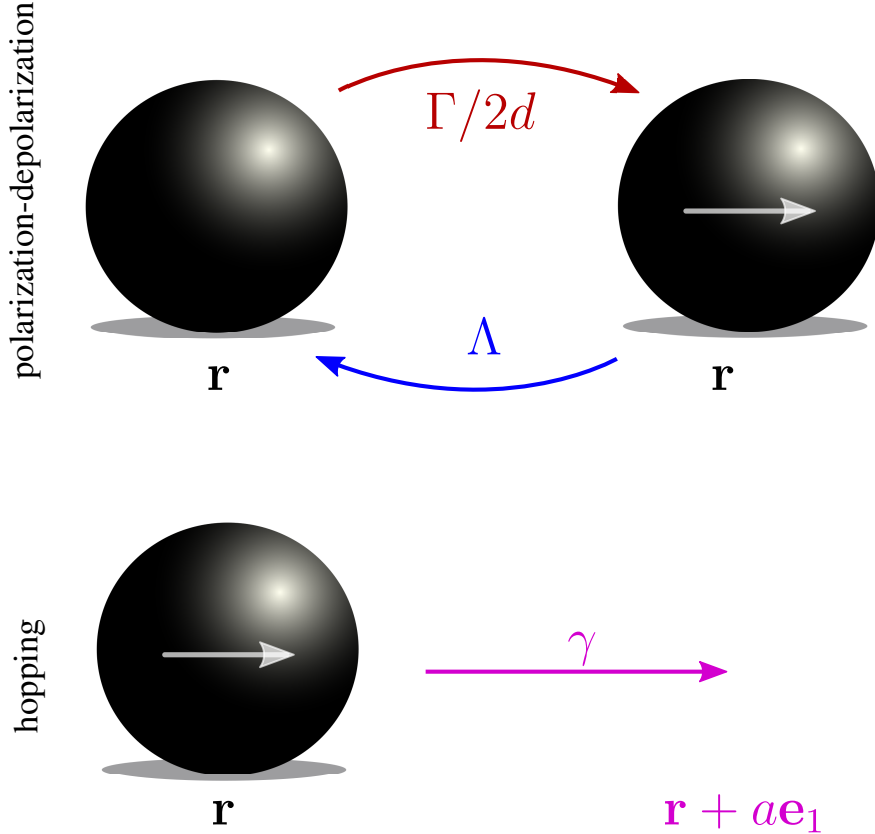


FIG. 1. Discrete model. Point-like objects represent cells located at the sites of periodic lattice with spacing a . (top) Cells polarize in a given direction with rate $\Gamma/2d$ and return to the non-polarized state with rate Λ . (bottom) Displacement to empty neighbouring sites occur with rate γ in the same direction of the cellular polarization.

$\delta t = 1/(\Lambda + \gamma)$ so that all transition probabilities involve only the ratios between Λ , γ , and Γ . The choice to tune δt based on transitions of polarized cells comes from observing that, in general, displacements are more common than morphological changes, $\gamma > \Gamma, \Lambda$. Alternatively, another common choice takes into account all transitions rates with equal footing, namely, $\delta t = 1/(\gamma + \Lambda + \Gamma)$ which tend to be more useful for general parameter regimes but may requires more steps to reach equilibrium. Regardless, the choice has no influence on the final results as long as one keeps track of δt .

Before moving on to the next section, we mention that the assumption of constant transition rates disregards the natural variability found in cells. Unlike self-propelled robots and Janus spheres [22, 39, 40], where parameters are strictly controlled, cells age and exhibit different morphological characteristics. As a result, the distribution of transition rates depend

on specific characteristics of individual cells. Cellular heterogeneity may break the assumption of Poisson processes depending on the magnitude of the variance and number of modes present in the distributions. A remedy to this issue contemplates grouping sub-populations of cells sharing the same physiological characteristics [41]. In our study, we assume cells belong to the same sub-population and share the same age.

II. THE MASTER EQUATION

Let $\rho_k(\mathbf{r}, t) \equiv \rho_k(\mathbf{r})$ be the instantaneous density of cells with polarization \mathbf{p}_k at the site \mathbf{r} , and $\rho_0(\mathbf{r}, t) \equiv \rho_0(\mathbf{r})$ the density of non-polarized cells. The local cell density $\rho(\mathbf{r}, t) = \sum_{k=-d}^d \rho_k(\mathbf{r}, t)$ describes the occupation at (\mathbf{r}, t) regardless of the polarization status and it is generally easier to extract from still images. In addition, the total number of cells $N = \sum_{\mathbf{r}} \rho(\mathbf{r}, t)$ is a conserved quantity in the automaton. According to the transition rules described in the previous section, and using the usual mean-field-like approximation that the presence or absence of cells on two distinct lattice sites are statistically independent (spatial correlations are neglected [35]), the master equations read

$$\partial_t \rho_0(\mathbf{r}) = -(\Gamma + \Lambda)\rho_0(\mathbf{r}) + \Lambda\rho(\mathbf{r}), \quad (1a)$$

$$\partial_t \rho_k(\mathbf{r}) = \gamma[1 - \rho(\mathbf{r})]\rho_k(\mathbf{r} - a\mathbf{e}_k) - \gamma[1 - \rho(\mathbf{r} + a\mathbf{e}_k)]\rho_k(\mathbf{r}) - \Lambda\rho_k(\mathbf{r}) + \frac{\Gamma}{2d}\rho_0(\mathbf{r}), \quad (1b)$$

for $k \neq 0$. Simultaneous occupation of sites is excluded by factors $1 - \rho(\mathbf{r})$. Note that the density of non-polarized cells (1a) lacks contributions from spatial displacements and, thus, only involves linear terms: it either increases due to the decay of polarized cells or decreases by transforming into them. In fact, the total number of non-polarized cells $N_0(t)$ satisfies $(d/dt)N_0 = -(\Gamma + \Lambda)N_0 + \Lambda N$ whose solution reads $N_0(t) = N/(1 + \Gamma/\Lambda) + ce^{-t/\tau_0}$ with characteristic relaxation time $\tau_0 = 1/(\Gamma + \Lambda)$. The constant c depends on initial conditions whereas the asymptotic value $N/(1 + \Gamma/\Lambda)$ represents the number of non-polarized cells in the equilibrium. Fig. 2 shows the evolution of the ratio N_0/N scaled by the factor $(1 + \Gamma/\Lambda)^{-1}$ for $\Gamma/\gamma = 1/2$, and $\Lambda/\gamma = 0.1$ or 0.001 . In both cases, the initial condition encompasses $N_1(0) = N$. Cells with lower depolarization rates remain polarized for longer periods which effectively reduces the asymptotic number of non-polarized cells. The scaling factor correctly captures the equilibrium value so that both curves converge to unity. However, the curves only overlap around the equilibrium value suggesting different relaxation times, as indicated

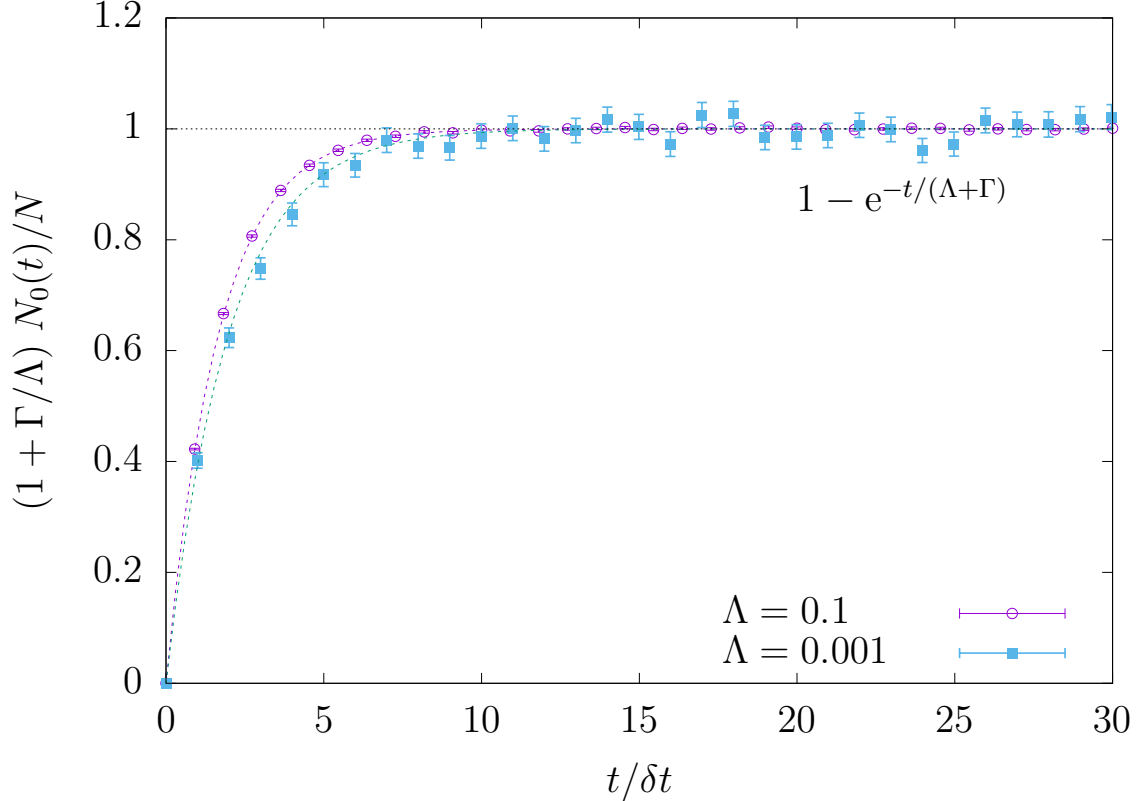


FIG. 2. Average scaled fraction of non-polarized cells along time for distinct values of depolarization rate. The parameters are $\Gamma = 1/2$, $\gamma = 1$, $L^2 = 64 \times 64$, $N = 100$, with 10^4 Monte Carlo samples. Superimposed curves (dashed lines) with relaxation time $\tau_0 = (\Lambda + \Gamma)^{-1}$.

by the superimposed dashed curves $1 - e^{-(\Gamma+\Lambda)t}$, in good agreement the theoretical predictions for τ_0 . Of course, the results for the total number of non-polarized cells should not present any surprise since in practice it describes a linear problem without any kind of spatial correlation.

The master equations (1a) and (1b) describe the stochastic dynamics of polarized cell and are thus subjected to fluctuations. The equivalent equations for the mean values $\langle \rho_k(\mathbf{r}) \rangle$ are obtained by averaging the equations over an ensemble of independent replicas. The procedure leads to contributions $\langle \rho_k(\mathbf{r}) \rho(\mathbf{r} \pm a\mathbf{e}_k) \rangle$ which includes two-point spatial correlations between neighbouring sites. It turns out that the dynamical equations for two-points correlations depend on three-points correlations, while the equivalent equation for three-points correlations requires inputs from 4-points correlations, etc. In short, the displacement of polarized cells form a set of hierarchical equations for correlations which only ends at N -

points. Instead of solving the complete set of equations one can gain valuable insights on the movement of polarized cells by studying the problem in the low density regime, where cells are likely uncorrelated due to the absence of long-range interactions. A coarse estimate of correlations is given by the mean-field approximation $\langle \rho_k(\mathbf{r})\rho(\mathbf{r} \pm a\mathbf{e}_k) \rangle \approx \langle \rho_k(\mathbf{r}) \rangle \langle \rho(\mathbf{r} \pm a\mathbf{e}_k) \rangle$ which neglects fluctuations entirely. Note that the mean-field approximation does not affect correlations involving the cellular polarization as in absence of additional cell-cell interactions they are only affected by the depolarization rate. In what follows, we drop the angular brackets to simplify the notation.

In addition to the mean-field approximation, it is convenient to introduce two new sets of variables derived from $\rho_k(\mathbf{r}, t)$ that capture the isotropic nature of the procedure that select new polarization states. This property ensures that, in practice, the local cell densities exhibit reflection and rotation symmetries once the distribution of polarization states reaches its equilibrium regime, characterized by the short relaxation time τ_0 (see Fig. 2). Thus, the density $\phi_k(\mathbf{r}, t) \equiv \phi_k = \rho_k + \rho_{-k}$ and the corresponding polarization current density $J_k(\mathbf{r}, t) \equiv J_k = \gamma(\rho_k - \rho_{-k})$ are more suitable quantities to describe the problem:

$$\partial_t \phi_k = -\Lambda \phi_k + \frac{\Gamma \rho_0}{d} - a \partial_k [(1 - \rho) J_k] + \frac{a^2 \gamma}{2} [(1 - \rho) \partial_k^2 \phi_k + \phi_k \partial_k^2 \rho] + \mathcal{O}(a^3), \quad (2a)$$

$$\partial_t J_k = -\Lambda J_k - a \gamma^2 \partial_k [(1 - \rho) \phi_k] + \mathcal{O}(a^2), \quad (2b)$$

with (1a) unchanged. One may further simplify (2a) and (2b) once enough time has passed to account for the repolarization of individual cells, $t \gg \tau_0$. The quasistatic approximation of (1a) gives $\phi_0(\mathbf{r}) = (1 + \Gamma/\Lambda)^{-1} \rho(\mathbf{r})$ while the isotropy of space ensures that on average ϕ_k behaves similarly in all directions, $\phi_k(\mathbf{r}) \approx (1/d) \sum_{m=1}^d \phi_m(\mathbf{r}) = d^{-1} (1 + \Lambda/\Gamma)^{-1} \rho(\mathbf{r})$. Combining (2a) for $k = 1, 2, \dots, d$ produces

$$\partial_t \rho = -a \nabla \cdot [(1 - \rho) \mathbf{J}] + \frac{a^2 \gamma}{2d} \left(\frac{1}{1 + \Lambda/\Gamma} \right) \nabla^2 \rho + \mathcal{O}(a^3), \quad (3a)$$

$$\partial_t \mathbf{J} = -\Lambda \mathbf{J} - \frac{a \gamma^2}{d} \left(\frac{1}{1 + \Lambda/\Gamma} \right) \nabla [(1 - \rho) \rho] + \mathcal{O}(a^2). \quad (3b)$$

The equation for total current $\mathbf{J}_T(t)$ can be obtained by integrating (3b) over the volume V and using the divergence theorem:

$$\frac{d\mathbf{J}_T}{dt} = -\Lambda \mathbf{J}_T - \frac{a \gamma^2}{d} \left(\frac{1}{1 + \Lambda/\Gamma} \right) \oint \rho(1 - \rho) d\mathbf{S}_d + \mathcal{O}(a^2). \quad (4)$$

For periodic boundary conditions, the surface integral vanishes and $|\mathbf{J}_T| = |\mathbf{J}_T(0)| e^{-\Lambda t}$ describes a simple decay process with relaxation time $\tau_1 = \Lambda^{-1}$. Fig. 3 depicts the evolution

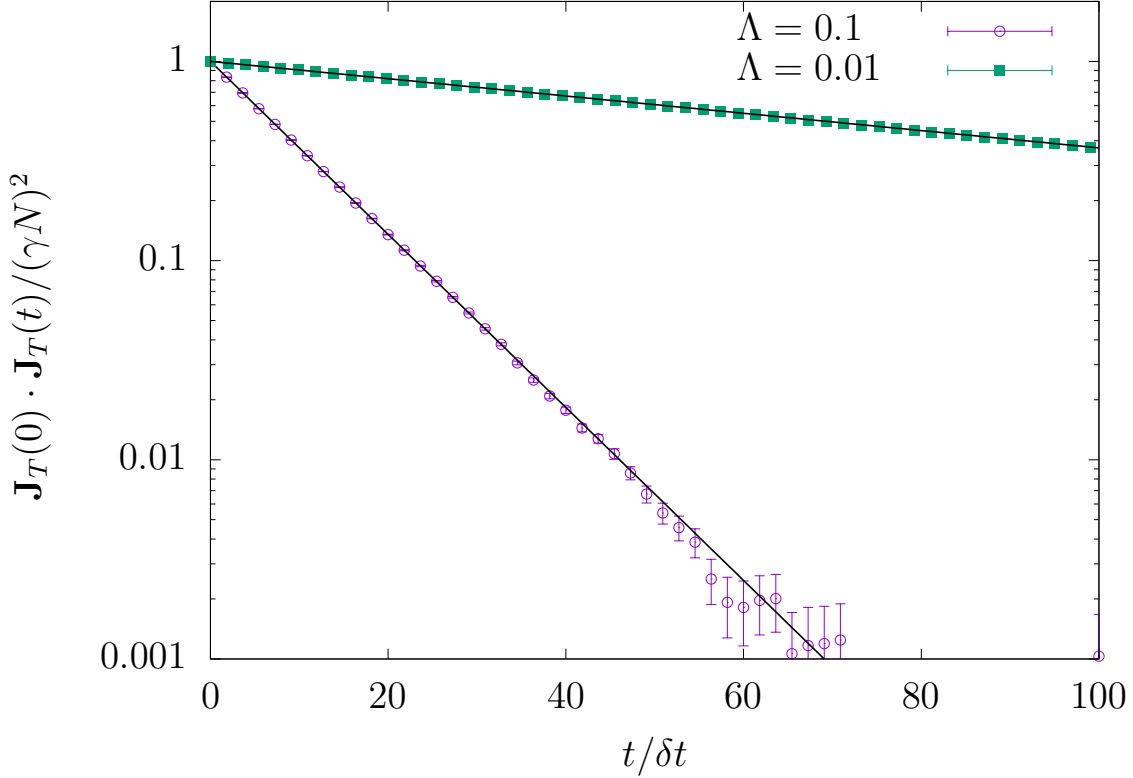


FIG. 3. Projection of the instantaneous total current $J_T(t)$ on $J_T(0)$. The parameters are $N = 100$, $L = 64$, $\Gamma = \gamma/2$ for $\Lambda/\gamma = 0.1$ (circles) or 0.01 (filled squares) in logscale, with 10^4 Monte Carlo samples. The solid lines are given by $\exp(-\Lambda t)$. 50% of the data is omitted for clarity.

of the total current for distinct depolarization rates $\Lambda/\gamma = 0.1$ and 0.01 , with the remaining parameters the same as in Fig. 2 and initial condition $\mathbf{J}_T(0) = \gamma N \mathbf{e}_1$. The solid lines are given by $e^{-\Lambda t}$ and show good agreement with the simulated data. Deviations between the curves and data become more significant as $|\mathbf{J}_T|/\gamma N$ approaches the typical error $1/\sqrt{M}$ associated with M independent Monte Carlo samples.

III. CLUSTER FORMATION

Although there are spatial contributions in (3a) and (3b), the global quantities N_0 and J_T are described solely in terms of the polarization-depolarization transitions. Translation symmetries often mask contributions coming from the various lattice sites so the local equations for cellular density require a more careful examination. In fact, local spatial correlations appear not only with increasing N but also with decreasing values of Λ as the persistence of cellular migration eventually creates long-lasting collisions between different cells. Fig. 4

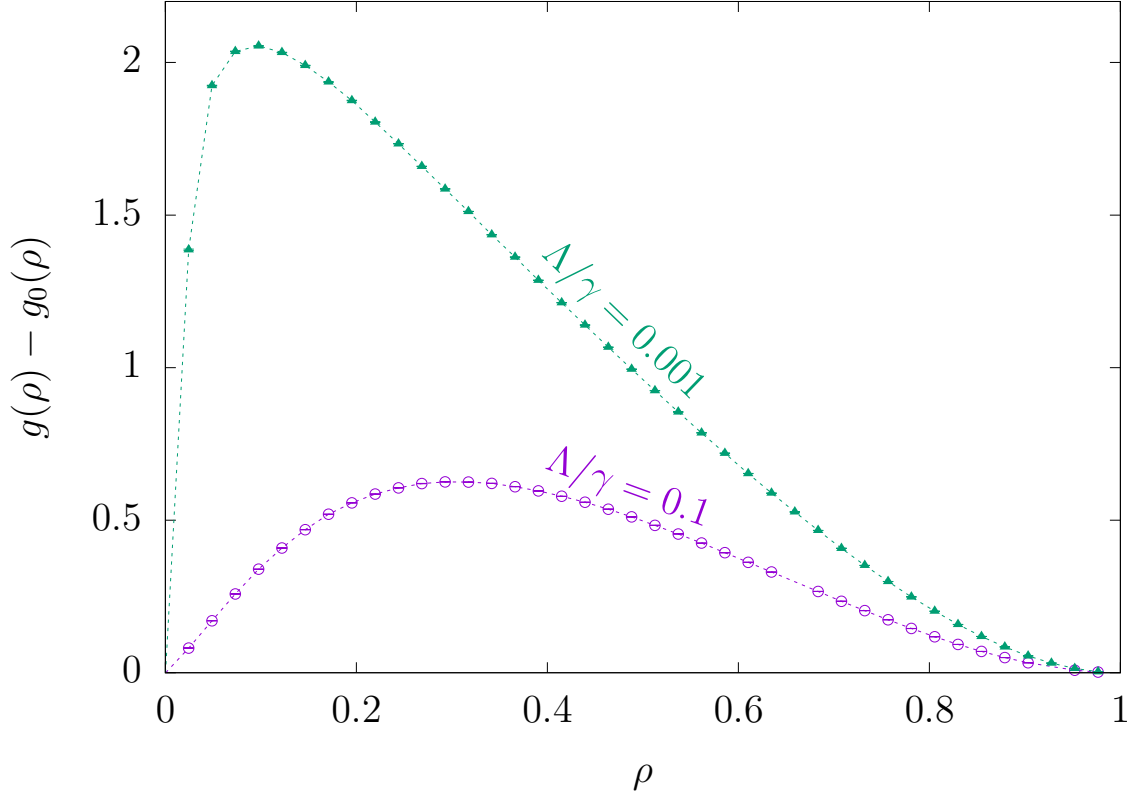


FIG. 4. Deviation in the number of adjacent cells in the polarized cell model compared to the random walker in $2d$ ($V = 64^2, \Gamma/\gamma = 1/2$) for several levels of cell density.

shows the deviation of the average number of adjacent cells $g(\rho)$ in the polarization model in comparison with the uncorrelated random walker $g_0(\rho) = 2d\rho$ in a periodic square lattice, both in equilibrium. The average numbers of adjacent cells are obtained from the pair distribution which in turn maps the complete spatial correlation between pairs. Thus, Fig. 4 shows that the system undergoes a dramatic change for vanishing Λ : cells tend to remain close to each other with enhanced spatial correlation and reduced mobility, violating the underlying hypothesis of the mean-field approximation.

Despite the lack of cohesive forces in the polarization model, cells may form long-lasting aggregates. Fig. 5 and Fig. 6 illustrate four instances of the polarization model in $d = 2$ with different values of $\Lambda/\gamma = 0.1$ and 0.001 , respectively, for different concentrations of cells. After a long transient (5×10^4 steps), the spatial distribution of cells is recorded for each instance and averaged over time (left column, Fig. 5 and Fig. 6). For $\Lambda/\gamma = 0.1$

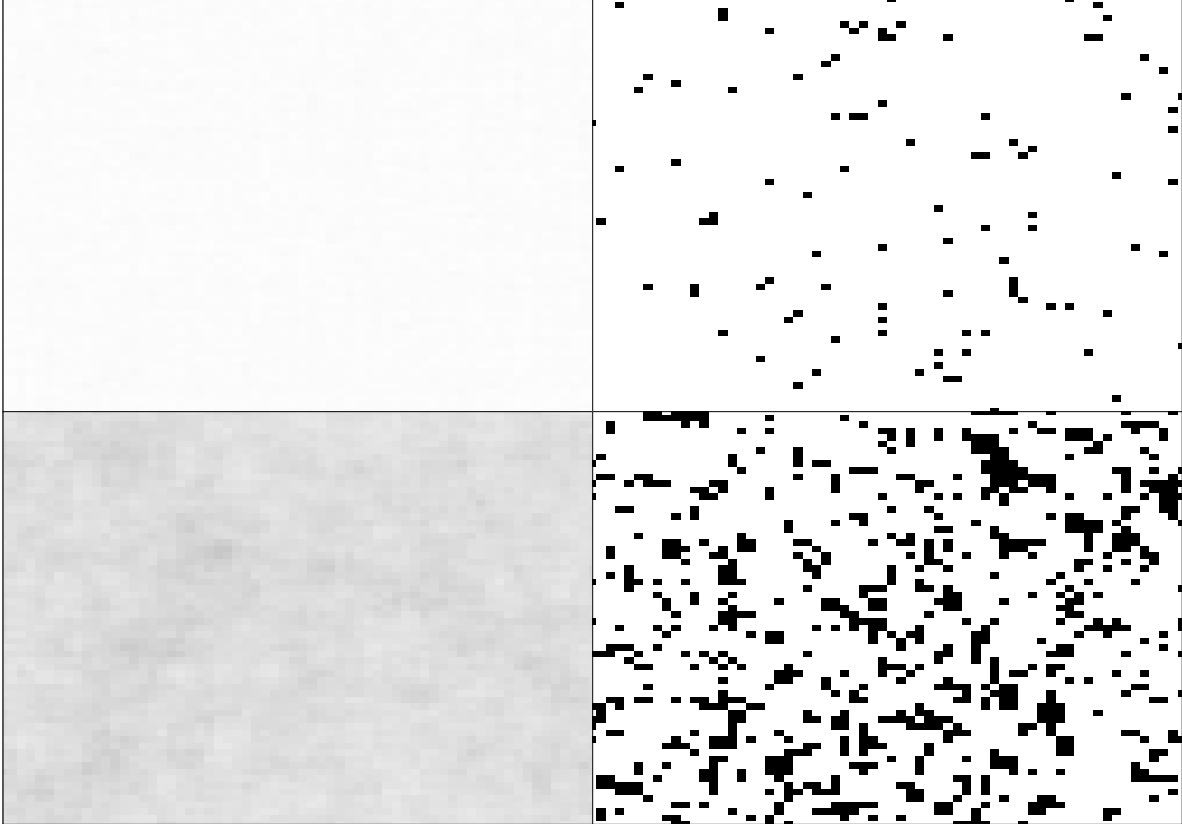


FIG. 5. Cellular aggregation for large depolarization rate. Time average of cell distributions over 10^4 samples (left column) with corresponding configuration snapshots (right column). $\Lambda/\gamma = 0.1$ with $N = 100$ cells (top) and $N = 800$ (bottom). Parameters $V = 64^2$, $\Gamma/\gamma = 1/2$ and samples collected after 5×10^4 steps.

the spatial distribution closely resembles the uniform distribution. Small clusters eventually form but they quickly break apart owing to their high depolarization-polarization rate. This mechanism ensures the complete visitation of the lattice and preserves the complete translation symmetry of the system. However, low depolarization rates $\Lambda/\gamma = 0.001$ promotes the formation of stable clusters. Cells along the cluster boundaries are still allowed to escape and dictate the equilibrium condition, namely, the regime in which the average number of departing and arriving cells are equal or, equivalently, a vanishing exchange current between the aggregated and isolated cells.

It is entirely reasonable to link cellular migration with cluster dynamics and related statistics (e.g. surface area, perimeter, and centroid). In exchange, one must obtain new master equations for the target cluster statistics that might or might not be derived from

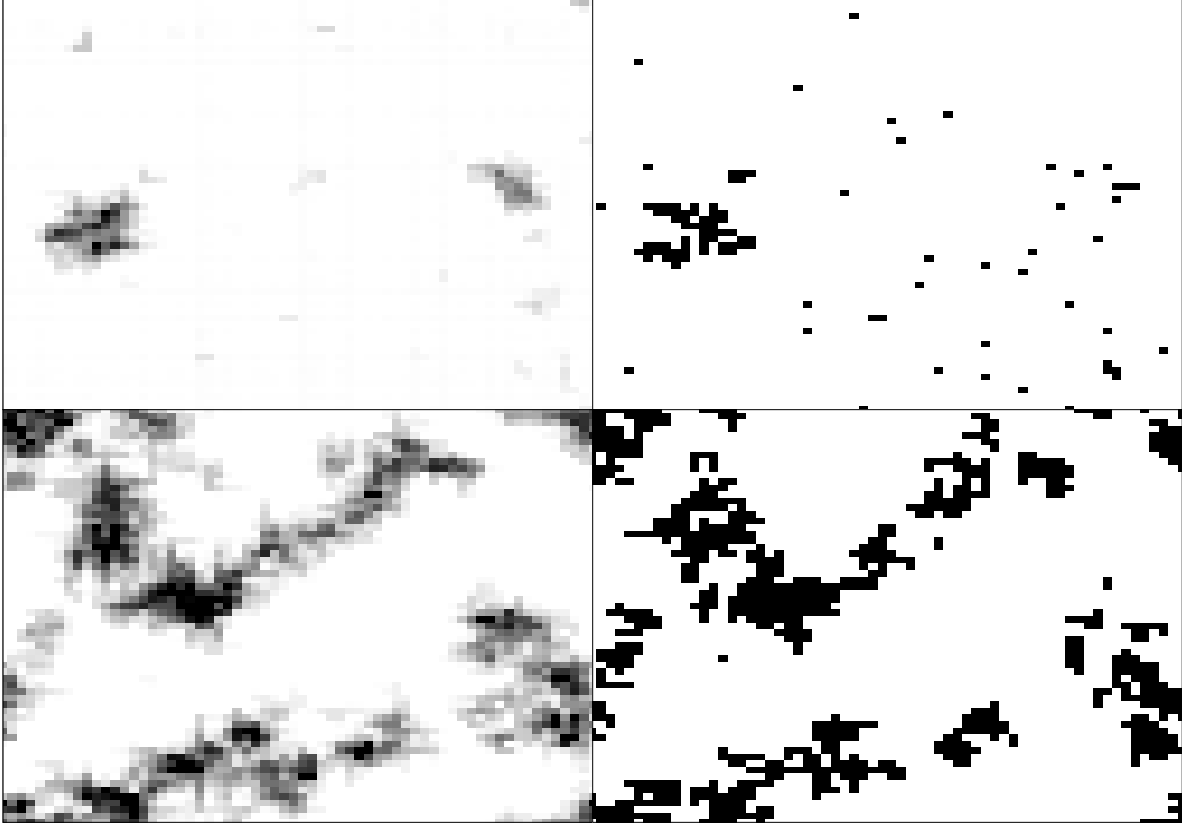


FIG. 6. Cellular aggregation for low depolarization rate. Time average of cell distributions over 10^4 samples (left column) with corresponding configuration snapshots (right column). $\Lambda/\gamma = 0.001$ with $N = 100$ cells (top) and $N = 800$ (bottom). Parameters $V = 64^2, \Gamma/\gamma = 1/2$. Samples collected after 5×10^4 steps.

(3a) and (3b). The problem with this approach stems from the fact that we only know the basic stochastic rules that govern the movement of cells, not their collective behavior. We avoid the search for new equations and instead introduce two familiar quantities to study the system, namely,

$$R^2(t_k) \equiv \left| \sum_{\ell=0}^k \sum_{m=1}^N [\mathbf{r}_m(t_{\ell+1}) - \mathbf{r}_m(t_{\ell})] \right|^2, \quad (5a)$$

$$S^2(t_k) \equiv \frac{1}{N} \sum_{m=1}^N |\mathbf{r}_m(t_{k+1}) - \mathbf{r}_m(t_k)|^2. \quad (5b)$$

$R^2(t)$ is simply the squared displacement or, alternatively, the square integrated velocity $R^2(t_k) = \delta t^2 \sum_{\ell, \ell'}^k \sum_{m, m'}^N \mathbf{v}_m(t_{\ell}) \cdot \mathbf{v}_{m'}(t_{\ell'})$. The average $\langle R^2 \rangle$ thus measures the collective dispersion of cells and involves the autocorrelation between cell velocities. For particles with

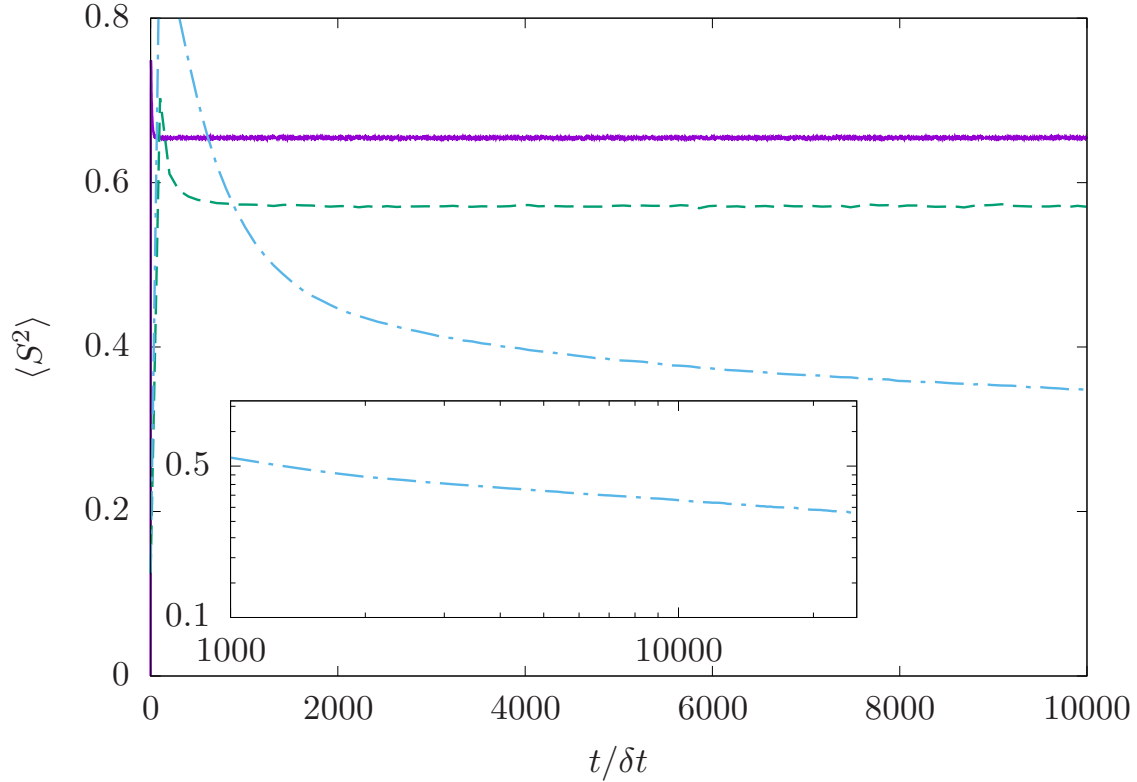


FIG. 7. Average one-step square displacement per particle. $V = 64^2$, $\Gamma/\gamma = 1/2$, $N = 100$ and 10^4 Monte Carlo samples. Average one-step square displacement $\langle S^2 \rangle$ equilibrates within times of the order of a few thousand steps for cluster-free configurations $\Lambda/\gamma = 0.1$ and 0.01 (— and -- respectively) but decays much more slowly, as an apparent power-law for $\Lambda/\gamma = 0.001$ (- · -). (inset) log-log scale.

negligible autocorrelation times one observes a regular diffusive behavior $\langle R^2(t) \rangle \approx (2dN)Dt$ expressing the relationship between $\langle R^2 \rangle$ and the diffusion coefficient D [42].

In all cases, cells experiment an explosive initial dispersion – owing to movement persistence – followed by a rapid decrease of the dispersion rate throughout the lattice. The phenomenon begins shortly after a time interval τ_1 has passed due to depolarization and it is enhanced by plastic collisions between cells. A portion of these collisions disrupt the cellular flow across the lattice producing a surge in the rigidity of the system (self-jamming effect). In practice, the presence of jams shift the tissue to a more liquid-like behavior. The transition from gas to liquid is one example of jamming transitions, which are believed to play an important role in tumor development and metastasis [43] and epithelial-to-mesenchymal transition [44]. For vanishing ratios Λ/γ , the longer persistence of cellular displacement

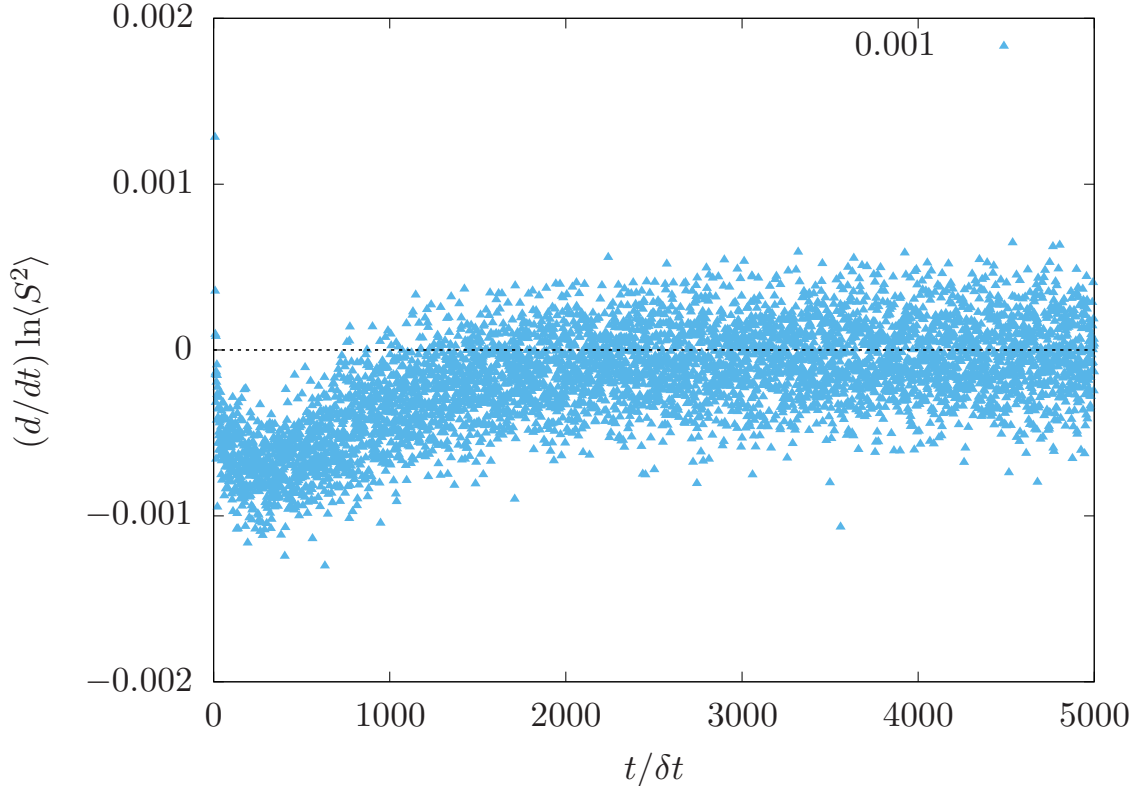


FIG. 8. Relative variation of one-step square displacements. $V = 64^2, \Gamma/\gamma = 1/2, N = 100$ and 10^4 Monte Carlo samples with $\Lambda/\gamma = 0.001$.

enhances the duration of jams, which in practice become nucleation centers for clusters. These special structures act as barriers that entrap arriving particles and may include up to $\mathcal{O}(N)$ cells. Once clusters are in place, the slope of $\langle R^2(t) \rangle$ is governed by the displacement of their peripheral cells as well as the relative few unbounded ones. The former encodes the fluctuations of departing and arriving particles into clusters as indicated by the light-gray regions at cluster boundaries in Fig. 6.

The behavior of fluctuations generally differs from the bulk counterpart and it is often accompanied by the emergence of power-laws [45]. Here, this behavior is captured by the average one-step square displacement $\langle S^2(t) \rangle$ as shown in Fig. 7. More specifically, $\langle S^2(t) \rangle$ decays as a power-law for vanishing Λ/γ in sharp contrast with the constant behavior observed in cluster-free configurations. In practice, plastic collisions reduce the overall displacement rate while cells escaping from clusters increase it, creating an out-of-equilibrium steady state. We can obtain a better assessment of equilibrium, or quasi-equilibrium for a lack of a better word, by using the relative variation $(d/dt) \ln \langle S^2(t) \rangle$, which fluctuates

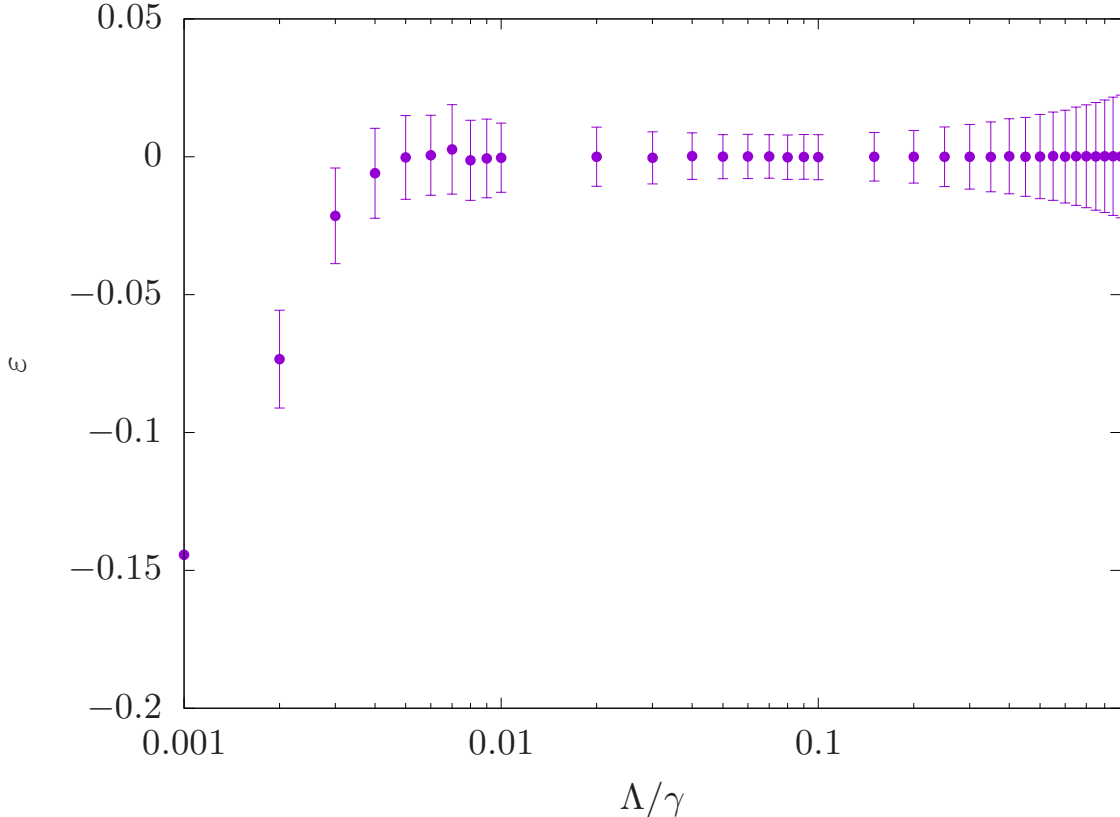


FIG. 9. Order parameter. The escape rate ε vanishes in the cluster-free regime. $N/V = 100/64^2$, $\Gamma/\gamma = 0.5$.

around zero once the bulk part of clusters is in place as depicted in Fig. 8. Here the derivative is computed as a forward derivative over one discrete time step.

We can exploit the effective power-law to define the escape rate $\varepsilon = \partial \ln \langle S^2 \rangle / \partial \ln t$ which vanishes in the free particle regime or acquires a non-null value in the cluster phase. The values that ε can assume in the cluster phase depend on the various transition rates (γ , Γ and Λ) and concentration N/V . Fig. 9 depicts an example for various values of Λ . As expected, $\varepsilon = 0$ in the free-particle phase but acquires negative values for some $\Lambda < \Lambda'$ indicating the emergence of clusters. In Fig. 9, we find that $\partial \varepsilon / \partial \Lambda$ diverges for vanishing Λ if the relation $\varepsilon \sim \ln \Lambda / \gamma$ holds.

IV. NON-LINEAR DIFFUSION IN THE DILUTED REGIME

The self-organization of polarized cells into long-lasting clusters shifts the description of the problem of microscopic entities (cells) to macroscopic ones (clusters). This occurs be-

cause the collective movement of cells in a given cluster can be perceived as the movement of the cluster itself. However, the macroscopic equations are not immediately obvious or known a priori unlike their microscopic counterparts. Phenomenological equations are good candidates to tackle the macroscopic approach but might require additional phenomenological parameters in order to address the various sorts of interactions that might arise.

We circumvent the issue altogether by studying the regions located far away from cluster boundaries. Because clusters capture surrounding particles, the remaining regions become deprived of cells and can be treated as a diluted phase. We refer to Fig. 6 where the emergence of clusters causes a dramatic reduction of migrating cells when compared to configurations with higher depolarization rates. Clusters describe a liquid-like phase whereas the surrounding regions populated by N' cells represent a diluted gas phase. As a result, only weak correlations survives between $N' < N$ cells in the diluted gas phase which in turn satisfies the requirements imposed by the mean-field equations (3a) and (3b).

With the above considerations in mind, we can obtain estimates for the local diffusion coefficient in the diluted gas phase. For that purpose, it is convenient to rewrite (3a) provided the quasistatic approximation $\mathbf{J} \approx -(a\gamma^2/d\Lambda)(1 + \Lambda/\Gamma)^{-1}(1 - 2\rho)\nabla\rho$, obtained from (3b) with $t \gg \tau_1$. Plugging the quasistatic approximation for \mathbf{J} into (3a) produces

$$\partial_t \rho = \frac{\gamma a^2}{2d} \left(\frac{\Gamma}{\Gamma + \Lambda} \right) \nabla \cdot \left[1 + \frac{2\gamma}{\Lambda} (1 - \rho)(1 - 2\rho) \right] \nabla \rho. \quad (6)$$

Starting from the continuity equation, one quickly identifies the cell current $\mathbf{j}_{\text{eff}} = -D_{\text{eff}}\nabla\rho$, in close analogy with Fick law, with the effective diffusion coefficient

$$D_{\text{eff}} = \frac{\gamma a^2}{2d} \left(\frac{\Gamma}{\Gamma + \Lambda} \right) \left[1 + \frac{2\gamma}{\Lambda} (1 - \rho)(1 - 2\rho) \right]. \quad (7)$$

The local distribution of cells $\rho(\mathbf{r}, t)$ creates implicit spatial contributions for D_{eff} and thus (6) is classified as a non-linear diffusion equation. We can check the limit as ρ tends to 0 of the expression (7) using the average square displacement $\langle R^2 \rangle$ for a single particle. In this case, no correlations appear and the global diffusion coefficient D corresponds to the spatial average of D_{eff} . In practice, the spatial averaging of (7) simply replaces the local densities by the concentration of cells N'/V . For a single particle, $N' = N = 1$. Indeed, (7) is in excellent agreement with D as shown in Fig. 10.

Nucleation induced by cellular jams disrupts the flow of cells across the lattice leading to an overall reduction of migrating cells and circulating volume for gaseous particles. The

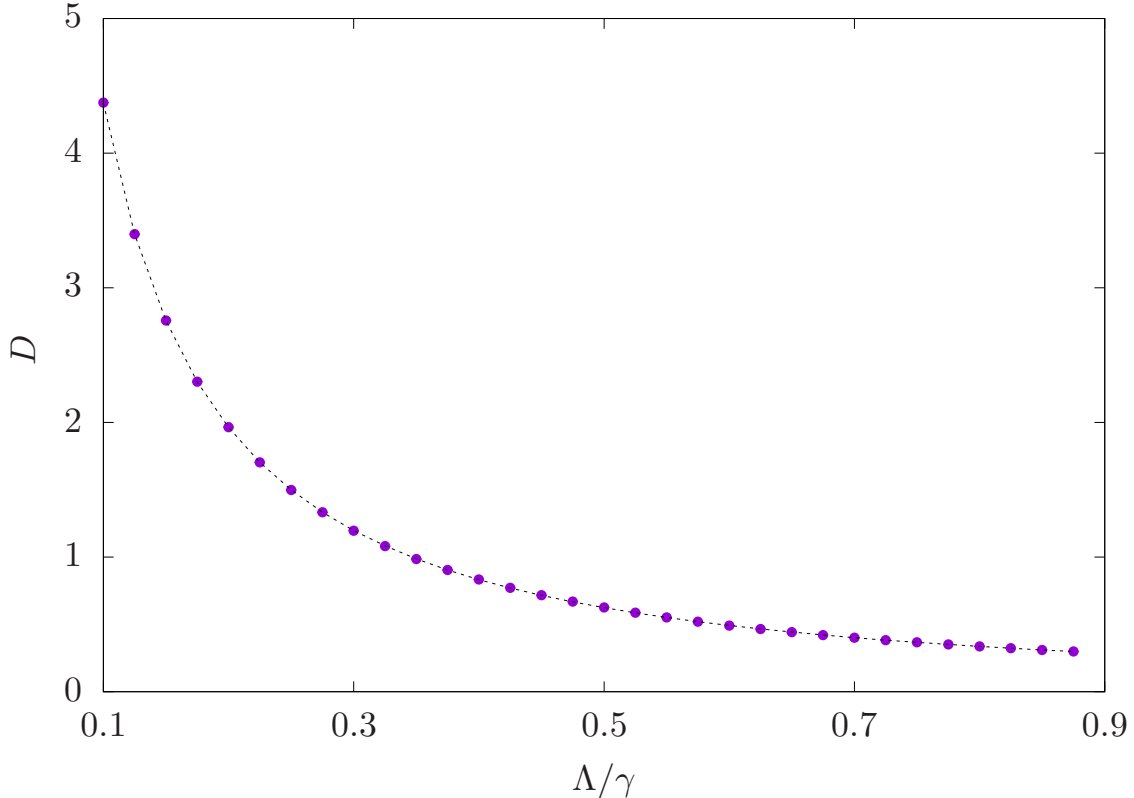


FIG. 10. Global diffusion coefficient per site for a single cell in the periodic square lattice. A least-square fitting procedure from the asymptotic behavior of $\langle R^2 \rangle \sim 4Dt$ extracts the global diffusion coefficient D (filled circles). The dashed line represents the spatial average of D_{eff} . Parameters $\Gamma/\gamma = 0.5$, $V = 64^2$ and 10^6 Monte Carlo samples.

accumulation of particles at nucleation sites creates regions with increased cell densities in which D_{eff} can take local negative values (see Fig. 11 dashed curve). This means that the local effective cell current $\mathbf{j}_{\text{eff}}(\mathbf{r}, t) = -D_{\text{eff}}\nabla\rho$ transport particles to high-density regions, contrary to the effective pressure caused by cell-cell exclusion. In addition, the average velocity and dispersion cells in these circumstances are locally reduced – they slow down around regions and tend to accumulate. This phenomenon drives the system towards MIPS. From a thermodynamical perspective, the co-existence of phase creates a concentration gradient supported by fast moving cells in one region and slow ones in the other [46, 47]. In a truly thermodynamical system, each region (bulk) would be treated as a particle reservoir with well-defined temperature with negligible boundary effects (surface). The equilibrium occurs when currents from and into the gas phase vanishes or, equivalently, when the competing

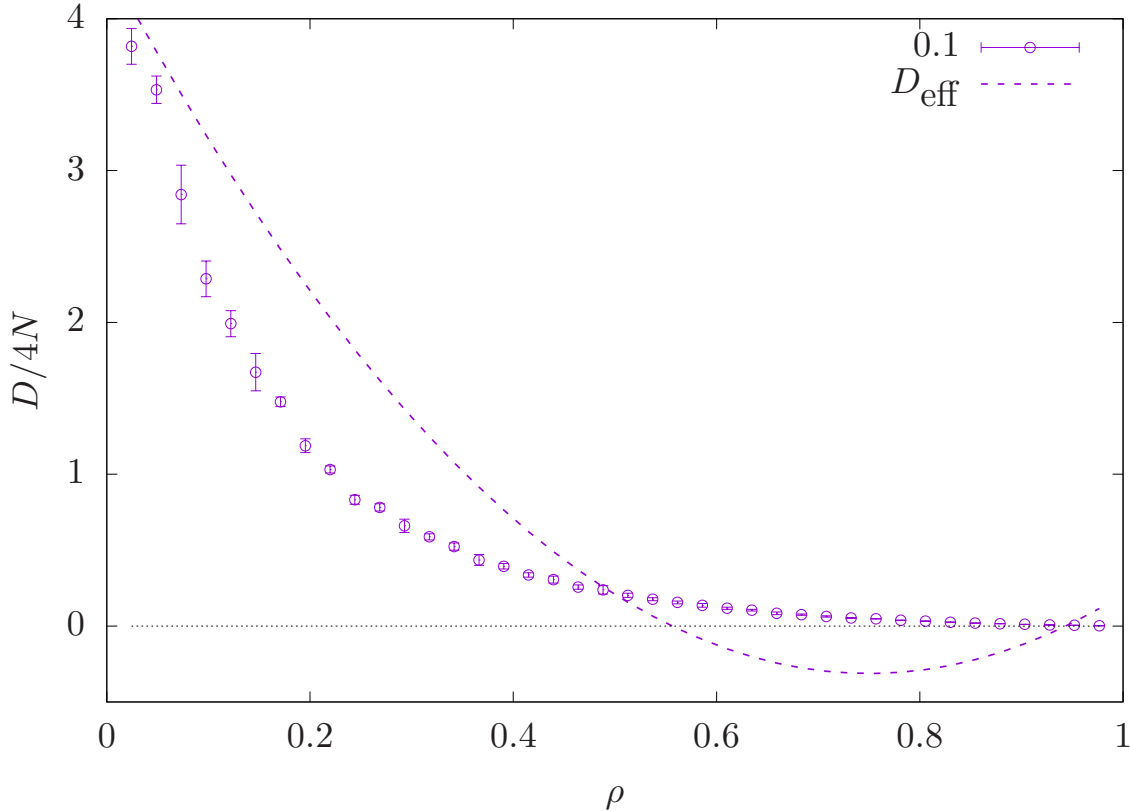


FIG. 11. Breakage of the mean-field approximation. Global diffusion coefficient (circles) extracted via the asymptotic least-square fitting $\langle R^2 \rangle \sim 4DNt$ for $\Lambda/\gamma = 0.1$, $V = 64^2$ and 10^4 Monte Carlo samples. The dashed curve represents D_{eff} .

chemical potentials match each other at phase interfaces.

For finite systems, exclusion and spatial correlations introduce deviations that break the mean-field approximation except for very low densities (see Fig. 11). In this case, boundary effects cannot be readily dismissed and a detailed analysis of correlations at gas-liquid interfaces becomes necessary, which lies well beyond the scope of this study. Instead we can understand general aspects of the gas phase by considering different estimates for N' while also neglecting eventual displacements that might occur within the cluster bulk.

As a first approximation, consider that the gas phase entails $N' = N_0$ isolated cells, i.e., cells without any neighbours. We compare the expected global diffusion $N_0 D_{\text{eff}}(N_0/V)$ with the asymptotic angular coefficient A obtained from $\langle R^2 \rangle$, for various cell densities. The results are shown in Fig. 12. For very low densities, we obtain good agreements for any depolarization regime as expected since the mean-field approximation holds. As the

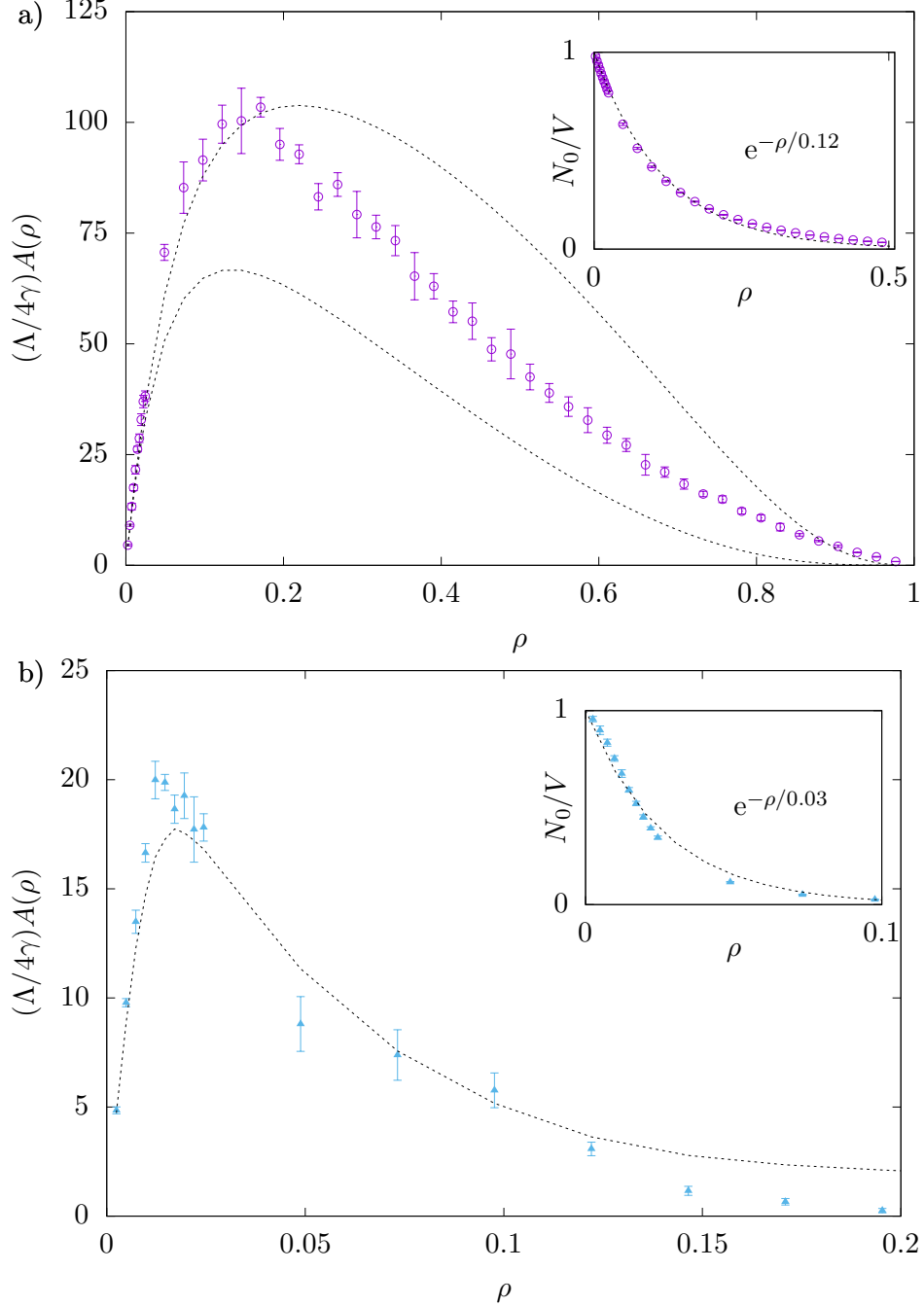


FIG. 12. Diffusion coefficients for high and low depolarization regimes. Scaled angular coefficient $A(\rho)$ obtained from asymptotic least-square fitting of $\langle R^2 \rangle \sim At$ for various cell densities. The dashed curves represent $(\Lambda/\gamma)N'D_{\text{eff}}(\rho')$ where $N' = \rho'V$ is the assumed number of particles in the gas phase. a) High depolarization regime $\Lambda/\gamma = 0.1$ and $N' = N_0$ ($N' = N_0 + N_1/2$) for the bottom (top) dashed curve. (inset) density of isolated cells decays exponentially. b) $\Lambda/\gamma = 0.001$ and $N' = N_0$.

density increases, collisions become more prominent and the behavior of the system changes depending on the depolarization regime. For high depolarization (low persistence) the curve for $N_0 D_{\text{eff}}(N_0/V)$ underestimates A (Fig. 12a bottom dashed line). However, the curve and the data share the same tendencies except in the interval of densities near their peaks. In practice this interval separates two distinct regimes of correlation between the $N_0 D_{\text{eff}}(N_0/V)$ and the data A . For lower densities, the ratio between the curves approaches unity. The ratio in the remaining interval produces a slow varying function that depends on N/V . This occurs because short-lived small clusters created by random collisions become more prominent as the density increases and they are not taken into account by N_0 . If we include particles with up to one neighbour $N' = N_0 + (1/2)N_1$ then the new curve overestimates the global diffusion of the system, as indicated by the top dashed curve in Fig. 12a). Here, N_1 is the number of particles with one neighbour and the factor $1/2$ is added to account for double counting. The correct value of N' lies in between both estimates and might include additional corrections from the particles with 2, 3 and 4 neighbours. Each of category of particle in respect to the number of cells changes differently according to the total number of particles in the system. The inset of Fig. 12a) shows how the density of isolated cells $\rho_0 \approx e^{-\rho/\rho_c}$ decays with the cell density with decay constant $\rho_c = 0.12$. In absence of persistence, the likelihood to find isolated cells should decay as $e^{-\rho/2d}$ for very low densities. This suggests that low persistence can produce observable effects to the aggregation rate even though the depolarization is not enough to foment stable nucleation sites.

We stress that our model disregards proliferation, which is what grants the malignant aspect of cancer cells. As a consequence, the removal of isolated particles indicated in the inset of Fig. 12 is expected at the start of the jamming transition. Empirical evidence for transformed MCF-10A mammary epithelial cells shows that the same phenomenon is observed in real cell systems [48]. The removal of dispersed individuals and adhesion to clusters results in a reduced proliferation rate due to contact inhibition. The coupling of both effects, cluster formation with contact inhibition, effectively reduces the number of isolated cells.

Figure 12b) depicts the scaled global diffusion in the low depolarization regime. In this case, the agreement between the simulated data and (7) with $N' = N_0$ (dashed line) is only seen at very low densities $\rho < 0.03$. After that, the scaled global diffusion quickly approaches zero whereas $(\Lambda/\gamma)N_0 D_{\text{eff}}(N_0/V)$ retains finite values. Extending $N' = N_0 + N_1/2$ do not

improve the agreement or trends. From the inset we can approximate the density of isolated cells ρ_0 by an exponential decay with decay constant $\rho_c = 0.03$ which means cells tends to strongly aggregate when compared to random Brownian particles. Unlike the previous case, and in light of the poor correlation between the scaled global diffusion coefficient and our estimates, coupled with the rapid depletion of isolated cells, one can conclude the gas phase ceases to exist past ρ_c . One possible explanation is that the mean-free path of the isolated cells is much shorter than the average distance between clusters so that they can be tracked down to cluster boundaries. The process describes the inter cluster exchange of isolated cells rather than exchange of cells between two phases in addition to their natural dynamics.

So far, we have not addressed the static properties of the clusters nor their implications to the particle dynamics. The static properties provide informative clues about the self-organization of particles into clusters and they have been extensively explored in the context of percolation and diffusion-limited aggregation [49]. The scale invariance observed for growing clusters also permits the analysis of anomalous scaling dimensions for specific metrics, which are often related to the types of interactions present in the system. Given the typical fractal-like morphology of the clusters (see Fig. 6) the scaling relation $n \propto R^{d_f}$ between the number of individuals in the cluster n and the gyration radius R is governed by the fractal dimension d_f .

The fractal dimension of polarized cells at fixed $N/V = 0.2$ and $\Lambda/\gamma = 0.001$ using the box counting method, $d_f = 1.47 \pm 0.04$. For reference, the fractal dimensions of the 2D self-avoiding walker and diffusion-limited aggregation sit at $4/3$ and ~ 1.7 , respectively. In that sense, our model would fall in between two processes with very dissimilar diffusion rules, namely, strong repulsion or irreversible adhesion, respectively. On grounds of fractal dimensions alone, our model is closer to random lattice animals whose fractal dimension is ~ 1.54 (Table I in [49]) for roughly disconnected clusters. In the random lattice animal model, clusters with varying shapes are placed at random in a lattice to produce configurations with fixed connection probability p [50]. If one does not fix p , the system converges exponentially towards equilibrium characterized by a random distribution of gaps [51].

One striking feature of polarized particles is their ability to aggregate (reversibly). In that regard, the large concentration of particles at cluster borders effectively removes isolated ones from the cluster surroundings, producing gaps in the spatial distribution. In practice, this simulates poorly connected percolation clusters ($p \rightarrow 0$). As pointed in [50], the random

lattice model exhibit conceptual similarities with clusters formed via Eden process, in which particles are added to a randomly selected perimeter site at each time step, starting from a single seed particle. Furthermore, the Eden process is also used to justify the emergence of non-linear terms in the famous KPZ equation for growing interfaces [52]. The expansion of (7) for vanishing densities produces $\partial_t \rho \approx A_1 \nabla^2 \rho - A_2 |\vec{\nabla} \rho|^2$ which is the averaged KPZ equation with constants $A_1 = D_0(1 + 2\gamma/\Lambda)$, $D_2 = 6D_0\gamma/\Lambda$, and $D_0 = (\gamma a^2/2d)\Gamma/(\Gamma + \Lambda)$. The equation can be further simplified using the transformation $\rho = -B \ln W(r, t)$ with $B = A_1/A_2$ so that one obtains the diffusion equation $\partial_t W = A_1 \nabla^2 W$. A noise term $\xi(t)$ can be added to describe the average arrival minus departure rate of particles at the interface of the clusters and thus recover the complete KPZ equation where $d = 2$ is the critical dimension with dynamical exponent $z = 3/2$.

For larger particle concentration N/V , the approximation no longer holds and non-linear terms proportional to ρ must be taken into account in the scaling analysis. Perhaps, more surprising is that the fractal dimension in the numerical simulations does not deviate too much from the values expected from the random lattice animals, suggesting the corrections are irrelevant for a certain range $(N/V, \Lambda/\gamma)$. A far more systematic investigation on the dependence of fractal dimensions with global parameters N/V and Λ/γ is beyond the scope of this study.

V. CONCLUSION

Active Brownian particles (ABP) systems display a number of unusual features and tend to self-organize into structures that might present relevant biological properties for living beings. Those features and structures are tied on how the ABP move and interact with each other and their surroundings. Among the myriad of types of movement performed by cells, directional persistence plays a major role in cell migration. In general, the directional persistence is dictated by chemotaxis but different scenarios arise that are not entirely explained by gradients of external molecules. That includes the migration of glioma cells that can even travel long distances in the brain. Although the ultimate goal of any ABP concerns the organization of biological elements, living beings might contain dozens or even hundreds of parameters and variables that might affect their displacement. To keep the analysis as tractable, one needs to reduce to set of parameters to the bare minimum that en-

closes the most significant factors. Here we consider a simple automaton in a square lattice that accounts for cell exclusion and directional persistence via the cellular polarization-depolarization process. We derive the master equation for the distribution of polarized cells and calculate the effective diffusion coefficient within the mean-field approximation. Despite the lack of adhesion forces in the model, our findings show the effective diffusion coefficient can acquire local negative values producing an effective current that transport cells from regions with low density of cell to rich ones. The process leads to self-jamming and favors the creation of nucleation sites, serving as an example of MIPS between clusters (liquid-like phase) and isolated cells (gas-like phase).

We also observe two regimes that can be characterized by the depolarization rate. In the high depolarization regime, self-jamming do not last long enough to facilitate aggregation. As a result, the system reaches equilibrium with constant asymptotic value for one-step square displacement $\langle S^2 \rangle$, and translation invariance is preserved as demonstrated by the uniform time-averaged distribution of cells across the lattice. Furthermore, the formula obtained for the effective diffusion coefficient for all isolated cells captures the general trends observed for the global diffusion coefficient of the system, with excellent agreement for low densities due to only small deviations from the mean-field approximation. Our findings also show that the directional persistence produces a non-negligible effect on the decay scale of the isolated cells.

In the low depolarization regime nucleation centers caused by self-jamming live long enough to support the organization of cells into large clusters. These structures can support a large portion of the cells in the system even at low concentrations. Unlike the previous regime, our results show an expressive disagreement between the global diffusion coefficient from the simulated data and our estimates using isolated cells, except for very low densities. Isolated cells are thus in-transit particles between the emission and respective arrival at cluster boundaries, driven entirely by surface effects and encoded by the escape rate ε . The phenomenon illustrates the effects of spatial correlations in the self-organization of ABP, and highlights the weakness in our approach since fluctuations are discarded in the mean-field approximation. Thus, a clear explanation of the phenomenology behind surface effects and spatio-temporal correlations becomes necessary to improve our understanding on the role

played by directional persistence in organization of active matter.

- [1] A. J. Koch and H. Meinhardt, “Biological pattern formation: from basic mechanisms to complex structures,” *Rev. Mod. Phys.* **66**, 1481–1507 (1994).
- [2] Fabien Gava, Bernard Ducommun, and Valérie Lobjois, “Anchorage-independent tumor cells clustering and implication in metastatic dissemination,” *Cancer. Ther. Oncol. Int. J.* **6** (2017).
- [3] Andrea Sottoriva, Joost J.C. Verhoeff, Tijana Borovski, Shannon K. McWeeney, Lev Naumov, Jan Paul Medema, Peter M.A. Slood, and Louis Vermeulen, “Cancer stem cell tumor model reveals invasive morphology and increased phenotypical heterogeneity,” *Cancer Res.* **70**, 46–56 (2010).
- [4] Peter Friedl and Darren Gilmour, “Collective cell migration in morphogenesis, regeneration and cancer,” *Nat. Rev. Mol. Cell. Biol.* **10**, 445–457 (2009).
- [5] Sophie Dekoninck and Cédric Blanpain, “Stem cell dynamics, migration and plasticity during wound healing,” *Nat. Cell Biol.* **21**, 18–24 (2019).
- [6] Christopher R. Cotter, Heinz-Bernd Schüttler, Oleg A. Igoshin, and Lawrence J. Shimkets, “Data-driven modeling reveals cell behaviors controlling self-organization during myxococcus xanthus development,” *Proc. Natl. Acad. Sci. USA* **114**, E4592–E4601 (2017).
- [7] Hannah Jeckel, Eric Jelli, Raimo Hartmann, Praveen K. Singh, Rachel Mok, Jan Frederik Tutz, Lucia Vidakovic, Bruno Eckhardt, Jörn Dunkel, and Knut Drescher, “Learning the space-time phase diagram of bacterial swarm expansion,” *Proc. Natl. Acad. Sci. USA* **116**, 1489–1494 (2019).
- [8] He Li, Xia-qing Shi, Mingji Huang, Xiao Chen, Minfeng Xiao, Chenli Liu, Hugues Chaté, and H. P. Zhang, “Data-driven quantitative modeling of bacterial active nematics,” *Proc. Natl. Acad. Sci. USA* **116**, 777–785 (2019).
- [9] Michalina Janiszewska, Marina Candido Primi, and Tina Izard, “Cell adhesion in cancer: Beyond the migration of single cells,” *J. Biol. Chem.* **295**, 2495–2505 (2020).
- [10] Shreyansh Jain, Victoire M. L. Cachoux, Gautham H. N. S. Narayana, Simon de Beco, Joseph D’Alessandro, Victor Cellerin, Tianchi Chen, Mélina L. Heuzé, Philippe Marcq, René-Marc Mège, and et al., “The role of single-cell mechanical behaviour and polarity in driving collective cell migration,” *Nat. Phys.* **16**, 802–809 (2020).

- [11] Andrew R. Houk, Alexandra Jilkine, Cecile O. Mejean, Rostislav Boltyskiy, Eric R. Dufresne, Sigurd B. Angenent, Steven J. Altschuler, Lani F. Wu, and Orion D. Weiner, “Membrane tension maintains cell polarity by confining signals to the leading edge during neutrophil migration,” *Cell* **148**, 175–188 (2012).
- [12] Jonathan E. Ron, Pascale Monzo, Nils C. Gauthier, Raphael Voituriez, and Nir S. Gov, “One-dimensional cell motility patterns,” *Phys. Rev. Res.* **2**, 033237 (2020).
- [13] Annette M. Molinaro, Jennie W. Taylor, John K. Wiencke, and Margaret R. Wensch, “Genetic and molecular epidemiology of adult diffuse glioma,” *Nat. Rev. Neurol.* **15**, 405–417 (2019).
- [14] Wanho Lee, Sookkyung Lim, and Yangjin Kim, “The role of myosin ii in glioma invasion: A mathematical model,” *PLOS ONE* **12**, e0171312 (2017).
- [15] Victoria Sanz-Moreno and Christopher J Marshall, “The plasticity of cytoskeletal dynamics underlying neoplastic cell migration,” *Curr. Opin. Cell Biol.* **22**, 690–696 (2010), cell-to-cell contact and extracellular matrix.
- [16] Naoyuki Inagaki and Hiroko Katsuno, “Actin waves: Origin of cell polarization and migration?” *Trends Cell Biol.* **27**, 515–526 (2017).
- [17] Ryan J. Petrie, Andrew D. Doyle, and Kenneth M. Yamada, “Random versus directionally persistent cell migration,” *Nat. Rev. Mol. Cell Biol.* **10**, 538–549 (2009).
- [18] Edward A Codling, Michael J Plank, and Simon Benhamou, “Random walk models in biology,” *J. R. Soc. Interface* **5**, 813–834 (2008).
- [19] J. Tailleur and M. E. Cates, “Statistical mechanics of interacting run-and-tumble bacteria,” *Phys. Rev. Lett.* **100**, 218103 (2008).
- [20] F. D. C. Farrell, M. C. Marchetti, D. Marenduzzo, and J. Tailleur, “Pattern formation in self-propelled particles with density-dependent motility,” *Phys. Rev. Lett.* **108**, 248101 (2012).
- [21] Alexandre P Solon, Joakim Stenhammar, Michael E Cates, Yariv Kafri, and Julien Tailleur, “Generalized thermodynamics of motility-induced phase separation: phase equilibria, laplace pressure, and change of ensembles,” *New J. Phys.* **20**, 075001 (2018).
- [22] F. Ginot, I. Theurkauff, F. Detcheverry, C. Ybert, and C. Cottin-Bizonne, “Aggregation-fragmentation and individual dynamics of active clusters,” *Nat. Commun.* **9**, 696 (2018).
- [23] Claudio B. Caporusso, Pasquale Digregorio, Demian Levis, Leticia F. Cugliandolo, and Giuseppe Gonnella, “Motility-induced microphase and macrophase separation in a two-

- dimensional active brownian particle system,” *Phys. Rev. Lett.* **125**, 178004 (2020).
- [24] Robert Großmann, Igor S. Aranson, and Fernando Peruani, “A particle-field approach bridges phase separation and collective motion in active matter,” *Nat. Commun.* **11**, 5365 (2020).
- [25] L. Caprini, U. Marini Bettolo Marconi, and A. Puglisi, “Spontaneous velocity alignment in motility-induced phase separation,” *Phys. Rev. Lett.* **124**, 078001 (2020).
- [26] Tamás Vicsek, András Czirók, Eshel Ben-Jacob, Inon Cohen, and Ofer Shochet, “Novel type of phase transition in a system of self-driven particles,” *Phys. Rev. Lett.* **75**, 1226–1229 (1995).
- [27] M. C. Marchetti, J. F. Joanny, S. Ramaswamy, T. B. Liverpool, J. Prost, Madan Rao, and R. Aditi Simha, “Hydrodynamics of soft active matter,” *Rev. Mod. Phys.* **85**, 1143–1189 (2013).
- [28] Fernando Peruani, Jörn Starruß, Vladimir Jakovljevic, Lotte Søggaard-Andersen, Andreas Deutsch, and Markus Bär, “Collective motion and nonequilibrium cluster formation in colonies of gliding bacteria,” *Phys. Rev. Lett.* **108**, 098102 (2012).
- [29] Bernard Derrida, “Non-equilibrium steady states: fluctuations and large deviations of the density and of the current,” *J. Stat. Mech.* **2007**, P07023–P07023 (2007).
- [30] William Bialek, Andrea Cavagna, Irene Giardina, Thierry Mora, Edmondo Silvestri, Massimiliano Viale, and Aleksandra M. Walczak, “Statistical mechanics for natural flocks of birds,” *Proc. Natl. Acad. Sci. USA* **109**, 4786–4791 (2012).
- [31] Andrea Cavagna, Luca Di Carlo, Irene Giardina, Luca Grandinetti, Tomas S. Grigera, and Giulia Pisegna, “Dynamical renormalization group approach to the collective behavior of swarms,” *Phys. Rev. Lett.* **123**, 268001 (2019).
- [32] Carl Merrigan, Kabir Ramola, Rakesh Chatterjee, Nimrod Segall, Yair Shokef, and Bulbul Chakraborty, “Arrested states in persistent active matter: Gelation without attraction,” *Phys. Rev. Res.* **2**, 013260 (2020).
- [33] Stephen Zhang, Aaron Chong, and Barry D. Hughes, “Persistent exclusion processes: Inertia, drift, mixing, and correlation,” *Phys. Rev. E* **100**, 042415 (2019).
- [34] M J Metson, M R Evans, and R A Blythe, “Jamming of multiple persistent random walkers in arbitrary spatial dimension,” *J. Stat. Mech.* **2020**, 103207 (2020).
- [35] Christophe Deroulers, Marine Aubert, Mathilde Badoual, and Basil Grammaticos, “Modeling tumor cell migration: From microscopic to macroscopic models,” *Phys. Rev. E* **79**, 031917 (2009).

- [36] Léo Adenis, Emilie Gontran, Christophe Deroulers, Basile Grammaticos, Marjorie Juchaux, Olivier Seksek, and Mathilde Badoual, “Experimental and modeling study of the formation of cell aggregates with differential substrate adhesion,” *PLOS ONE* **15**, e0222371 (2020).
- [37] Katherine Copenhagen, Gema Malet-Engra, Weimiao Yu, Giorgio Scita, Nir Gov, and Ajay Gopinathan, “Frustration-induced phases in migrating cell clusters,” *Sci. Adv.* **4** (2018), 10.1126/sciadv.aar8483.
- [38] Olga Iliina, Pavlo G. Gritsenko, Simon Syga, Jürgen Lippoldt, Caterina A. M. La Porta, Oleksandr Chepizhko, Steffen Grosser, Manon Vullings, Gert-Jan Bakker, Jörn Starruß, Peter Bult, Stefano Zapperi, Josef A. Käs, Andreas Deutsch, and Peter Friedl, “Cell–cell adhesion and 3d matrix confinement determine jamming transitions in breast cancer invasion,” *Nat. Cell Biol.* **22**, 1103–1115 (2020).
- [39] Julien Deseigne, Olivier Dauchot, and Hugues Chaté, “Collective motion of vibrated polar disks,” *Phys. Rev. Lett.* **105**, 098001 (2010).
- [40] Guillaume Briand, Michael Schindler, and Olivier Dauchot, “Spontaneously flowing crystal of self-propelled particles,” *Phys. Rev. Lett.* **120**, 208001 (2018).
- [41] David B. Brückner, Alexandra Fink, Joachim O. Rädler, and Chase P. Broedersz, “Disentangling the behavioural variability of confined cell migration,” *J. R. Soc. Interface* **17**, 20190689 (2020).
- [42] Nikolai V. Brilliantov and Thorsten Pöschel, “Self-diffusion in granular gases: Green–kubo versus chapman–enskog,” *Chaos* **15**, 026108 (2005).
- [43] Linda Oswald, Steffen Grosser, David M Smith, and Josef A Käs, “Jamming transitions in cancer,” *J. Phys. D Appl. Phys.* **50**, 483001 (2017).
- [44] Dapeng Bi, Xingbo Yang, M. Cristina Marchetti, and M. Lisa Manning, “Motility-driven glass and jamming transitions in biological tissues,” *Phys. Rev. X* **6**, 021011 (2016).
- [45] Qian-Yuan Tang, Yang-Yang Zhang, Jun Wang, Wei Wang, and Dante R. Chialvo, “Critical fluctuations in the native state of proteins,” *Phys. Rev. Lett.* **118**, 088102 (2017).
- [46] Juliane U. Klamsner, Sebastian C. Kapfer, and Werner Krauth, “Thermodynamic phases in two-dimensional active matter,” *Nat. Commun.* **9**, 5045 (2018).
- [47] Suvendu Mandal, Benno Liebchen, and Hartmut Löwen, “Motility-induced temperature difference in coexisting phases,” *Phys. Rev. Lett.* **123**, 228001 (2019).
- [48] Susan E. Leggett, Zachary J. Neronha, Dhananjay Bhaskar, Jea Yun Sim, Theodora Myrto

- Perdikari, and Ian Y. Wong, “Motility-limited aggregation of mammary epithelial cells into fractal-like clusters,” *Proc. Natl. Acad. Sci. USA* **116**, 17298–17306 (2019).
- [49] T. A. Witten and L. M. Sander, “Diffusion-limited aggregation, a kinetic critical phenomenon,” *Phys. Rev. Lett.* **47**, 1400–1403 (1981).
- [50] H. P. Peters, D. Stauffer, H. P. Hölters, and K. Loewenich, “Radius, perimeter, and density profile for percolation clusters and lattice animals,” *Z. Phys. B* **34**, 399–408 (1979).
- [51] I. Lončarević, Lj. Budinski-Petković, J. R. Šćepanović, Z. M. Jakšić, and S. B. Vrhovac, “Random sequential adsorption of lattice animals on a three-dimensional cubic lattice,” *Phys. Rev. E* **101**, 012119 (2020).
- [52] Mehran Kardar, Giorgio Parisi, and Yi-Cheng Zhang, “Dynamic scaling of growing interfaces,” *Phys. Rev. Lett.* **56**, 889–892 (1986).